Thermal transport analysis in hydromagnetic fluid-particle suspension model under the effect of slip boundary conditions and electric field: Applications in solar power plant

S. Saleem[1], Mubbashar Nazeer[2,*], M. Waqas Nazir[3], Leema Aliyaru Kunju[4]

[1]Department of Mathematics, College of Science, King Khalid University, Abha 61413, **Saudi Arabia**

[2]Department of Mathematics, Institute of Arts and Sciences, Government College University Faisalabad Chiniot Campus, 35400, **Pakistan**

[3]Department of Mathematics and Statistics, International Islamic University Islamabad, 44000 **Pakistan**

[4]Department of Mathematics College of Science, Jazan University, Jazan, **Saudi Arabia**

(Corresponding Author: mubbasharnazeer@gcuf.edu.pk)

Abstract

The objective of this study is to investigate the effects of heat transfer analysis on Casson fluid flow with the suspension of solid particles through divergent channels under the influence of magnetic force and slip boundary conditions. The governing equations of non-Newtonian fluid (i.e. Casson fluid) are solved and presented as the closed-form solution of the problem. The graphical behavior is constructed in MATHEMATICA software and discusses the effects of emerging parameters of the current study on fluid and particle velocities distribution, stream function, temperature profile, and heat transfer rate. The temperature distribution increases against the thermal slip parameter and decreases via the velocity slip parameter. The heat transfer rate is a decreasing function of the non-Newtonian parameter, velocity slip parameter, Hartman number, and coefficient of particle fraction while this behavior no longer exists against the thermal slip parameter, Brinkman number, the Helmholtz–Smoluchowski velocity, and electroosmotic parameter. The results of our study can be reduced to the Newtonian fluid by taking $N_p \to \infty$. The current fluid-particle suspension Casson model helps understand the thermal properties of such a model under the action of the electric and magnetic field with slip boundary conditions. Further, the suspension of dense particles can be useful in solar power plants to restore more energy.

Keywords: Hydromagnetic flow; fluid-particle phases; slip boundary conditions; Heat transfer analysis; closed-form solution.

1. Introduction

The theory of multiphase flow is extremely accommodated to understanding the physical phenomena of engineering environments namely, the production of cement, treatment of wastewater, manufacturing of the steel industry, lunar ash flow, gas purification, purification of crude oil production, paint spraying, transport process, dust collection, and environmental pollution motion [1-2], etc. The first work on the suspension of solid particles in viscous fluid was done by Saffman [3]. He reported the stability analysis of laminar dusty gas in his published book. After his study, various authors highlighted the importance of fluid and particle phases in diverse shapes of geometries. For this, Bhatti et al. [4] presented the clot blood model of fluid and particle phase suspension to report the heat transfer analysis in variable annulus under the effects of slip boundary conditions. The fluid and particle suspension through the ciliated walls of the porous channel under the action of magnetic force was investigated by Bhatti et al. [5].

Their outcomes revealed that the velocity distribution diminished via the magnetic force parameter. In another study, Bhatti et al. [6] used the Darcy-Brinkman-Forchheimer model to report the porous medium effects in bi-phase liquid by taking the Sisko non-Newtonian fluid. Nazeer et al. [7-9] discussed the suspension of solid particles in Jeffrey fluid, Couple Stress fluid, and third-grade fluid and presented some important results on multiphase fluids in different geometries. Kumar et al. [10] discussed the suspension of fluid and particles past a stretching surface with thermal radiation effects.

The flow of electrically conducting fluid under the suspension of solid particles has great applications in manufacturing industries such as polymer technology, the petroleum industry, cooling systems, MHD generators, centrifugal separation of matter from fluid and accelerators, etc. Many researchers and scholars have studied the suspension of solid particles in liquid under the effects of magnetohydrodynamics in different regions like flow through parallel plates, flow in wavy channels and stretching surfaces, etc., and with different boundary conditions. Pavithra and Gireesha [11] discussed the heat transfer analysis in fluid-particle suspension over a stretching sheet by using the numerical technique. Hatami et al. [12] selected the two moving parallel plates to discuss the fluid and particle suspension in a Newtonian fluid under the action of the magnetic field. Jha and Apere [13] presented the closed-form solution of the time-dependent fluid and particle phase model between two infinite plates. The Laplace transformation method is used to solve the governed problem and discusses the graphical behavior of both phase velocities. In another study, Jha and Malgwi [14] studied the hydro-magnetic unsteady flow of fluid through the moving wall of the porous channel. Al-Zubaidi et al. [15], Ge-JiLe et al. [16], Zeeshan et al. [17], Ellahi et al. [18], Bibi et al. [19], and Gad [20], etc. also presented the application of fluid and particle phase model under the effects of the magnetic field in the diverse shape of geometries.

The study of heat transfer in the suspension of solid particles has been attracted by scholars and researchers due to its wider applications in polymer processing technology, solar power plants, engine oil flow, and many others in well-known literature. Particularly, the applications of the MHD flow and heat transfer analysis of electrically conducting fluids with possible suspension of solid particles through channels and pipes occur in MHD generators and pumps, nuclear reactors, filtration, geothermal systems, etc. In the literature, Chamkha [21] formulated the continuum model of fluid and particle phases to analyze the heat transfer analysis in two different types of geometries (channels and pipes) under the effects of the magnetic field. The Fourier cosine and Bessel functions are used by him to obtain the closed-form solution of fluid and particle phases while the energy equation is solved through numerical methods. His results revealed that the flow and heat transfer is superior in the case of channels as compared to pipes. Ansart et al. [22] presented the applications of heat transfer analysis through gas-particle suspension in solar receivers by using the three-dimensional numerical technique. The application of dense particle suspension in thermal power plants was highlighted by Spelling et al. [23]. The applications of heat transfer rate along with slip boundary conditions, Darcy–Brinkman–Forchheimer porous medium, and magnetic field in fluid and particle phase models through the wavy channel were reported by Imran et al. [24]. Bhatti and Zeeshan [25] also reported the applications of heat transfer analysis in particle suspension by using the slip boundary conditions in peristaltic waves by considering the Casson fluid. Some authors have also presented remarkable studies of heat transfer analysis in the suspension of solid particles in different environments [26-30].

In view of the above-cited analyses, the objective of this study is to investigate the effects of heat transfer analysis on Casson fluid flow with the suspension of solid particles through the divergent channels under the influence of magnetic force and slip boundary conditions. To the best of our knowledge, no such study has been done before. Such type of flow problems are important in the human body where the heat transfer process is very important to maintain the feasible condition of tissues and circulation of the blood through arteries. Furthermore, these types of problems are also very useful and interesting in thermal technology where the dense suspension of the particle provides direct thermal storage due to the maximum heat capacity and greater temperature of particle suspension. Moreover, the regular heat transfer fluids used in thermal power plants have many serious drawbacks (i.e. working in a limited temperature domain), and solid suspension of particles overcomes these drawbacks as heat transfer fluids. The solid particles can also be used as an energy storage medium. The governed system equations are formulated by using the Poisson equation, continuity equation, momentum equation, and heat equations and offered the closed solution through MATHEMATICA software. The physical outcomes are interpreted through graphs and tables and presented as the important results.

2. Mathematical analysis

Let us consider the steady flow of Casson fluid suspended by 40 % Hafnium solid spherical particles in the divergent channel as shown in **Figure 1**. $\mathbf{V}_{fv} = \left[u_{fv}(\eta_1,\eta_2), v_{fv}(\eta_1,\eta_2), 0\right]$ and $\mathbf{V}_{pv} = \left[u_{pv}(\eta_1,\eta_2), v_{pv}(\eta_1,\eta_2), 0\right]$ are the velocity vectors of fluid and particulate.

Geometry:

$$h(\eta_1) = \begin{cases} a - b\sin^2\left(\dfrac{\pi\eta_1}{\xi}\right) & \text{When } \dfrac{11}{7} < \eta_1 < \dfrac{33}{7}. \\ 0.5a; & \text{Othwewise.} \end{cases} \quad (1)$$

2.1 The physical model of the fluid phase

The continuity and momentum equation for the fluid phase in vector form is defined [31-34] as

$$\frac{\partial \rho_f}{\partial t} + \nabla.\left(\rho_f \mathbf{V}_{fv}\right) = 0, \quad (2)$$

$$\rho_f\left(1-c_m\right)\frac{d\mathbf{V}_{fv}}{dt} = -\left(1-c_m\right)\nabla p + \nabla.\mathbf{T}_{ij} + D_f c_m\left(\mathbf{V}_{pv} - \mathbf{V}_{fv}\right) + \mathbf{J}\times\mathbf{B} + \nabla^2\Phi E_{\eta_p} + \rho_f g\,. \quad (3)$$

The extra stress tensor "T_{ij}" for the Casson fluid can also be expressed [35-36] as:

$$\mathbf{T}_{ij} = \begin{cases} 2\left(\mu_b + \dfrac{p_{\eta_2}}{\sqrt{2\pi}}\right)e_{ij}, & \pi > \pi_c \\ 2\left(\mu_b + \dfrac{p_{\eta_2}}{\sqrt{2\pi}}\right)e_{ij}, & \pi < \pi_c \end{cases}. \quad (4)$$

In the above mathematical expression $\mathbf{T}_{ij}$ is known as the $(i,j)^{th}$ components of the stress tensor, the plastic dynamic viscosity of a non-Newtonian fluid are denoted by μ_b, the yield stress of the fluid is p_{η_2}, e_{ij} is the $(i,j)^{th}$ components of deformation rate, π is expressed as $\left(\pi = e_{ij}e_{ij}\right)$ that is the product of components of deformation rate with itself, and π_c is called the deformation rate of non-Newtonian fluid.

2.2 The physical model of the particle phase

The continuity and momentum equation for the particle phase in vector form is defined as

$$\frac{\partial \rho_p}{\partial t} + \nabla.\left(\rho_p \mathbf{V}_{pv}\right) = 0, \tag{5}$$

$$\rho_f c_m \frac{d\mathbf{V}_{pv}}{dt} = -c_m \nabla p - D_f c_m \left(\mathbf{V}_{pv} - \mathbf{V}_{fv}\right). \tag{6}$$

To discuss the thermal transport analysis, the heat equation is expressed [37-38] as

$$\rho_f \left(c_p\right)_f \frac{dT_{f,p}}{dt} = K\nabla^2 T_{f,p} + \mu_s \phi\,. \tag{7}$$

The above equations are expressed in component form as

$$\frac{\partial u_{fv}}{\partial \eta_1} + \frac{\partial v_{fv}}{\partial \eta_2} = 0, \tag{8}$$

$$\left.\begin{aligned} &\rho_f (1-c_m)\left[\frac{\partial u_{fv}}{\partial t} + u_{fv}\frac{\partial u_{fv}}{\partial \eta_1} + v_{fv}\frac{\partial u_{fv}}{\partial \eta_2}\right] = -(1-c_m)\frac{\partial p}{\partial \eta_1} + \mu_s (1-c_m)\left(1+\frac{1}{N_p}\right)\left[\frac{\partial^2 u_{fv}}{\partial \eta_1^{\,2}} + \frac{\partial^2 u_{fv}}{\partial \eta_2^{\,2}}\right] \\ &+ D_f c_m \left(u_{pv} - u_{fv}\right) - \sigma B_0^2 u_{fv} + \left[\frac{\partial^2 \Phi}{\partial \eta_1^{\,2}} + \frac{\partial^2 \Phi}{\partial \eta_2^{\,2}}\right] E_{\eta_1} \end{aligned}\right\}, \tag{9}$$

$$\left.\begin{aligned} &\rho_f (1-c_m)\left[\frac{\partial v_{fv}}{\partial t} + u_{fv}\frac{\partial v_{fv}}{\partial \eta_1} + v_{fv}\frac{\partial v_{fv}}{\partial \eta_2}\right] = -(1-c_m)\frac{\partial p}{\partial \eta_2} + \mu_s (1-c_m)\left(1+\frac{1}{N_p}\right)\left[\frac{\partial^2 v_{fv}}{\partial \eta_1^{\,2}} + \frac{\partial^2 v_{fv}}{\partial \eta_2^{\,2}}\right] \\ &+ D_f c_m \left(v_{pv} - v_{fv}\right) - \sigma B_0^2 v_{fv} + \left[\frac{\partial^2 \Phi}{\partial \eta_1^{\,2}} + \frac{\partial^2 \Phi}{\partial \eta_2^{\,2}}\right] E_{\eta_2} \end{aligned}\right\}, \tag{10}$$

$$\rho_f (c_p)_f \left[\begin{aligned} &\frac{\partial T_{f,p}}{\partial t} + u_{fv}\frac{\partial T_{f,p}}{\partial \eta_1} \\ &+ v_{fv}\frac{\partial T_{f,p}}{\partial \eta_2} \end{aligned}\right] = K\left[\frac{\partial^2 T_{f,p}}{\partial \eta_1^{\,2}} + \frac{\partial^2 T_{f,p}}{\partial \eta_2^{\,2}}\right] + \left(1+\frac{1}{N_p}\right)\left[\begin{aligned} &2\left(\frac{\partial u_{fv}}{\partial \eta_1}\right)^2 \\ &+2\left(\frac{\partial v_{fv}}{\partial \eta_2}\right)^2 + \left(\frac{\partial u_{fv}}{\partial \eta_2} + \frac{\partial v_{fv}}{\partial \eta_1}\right)^2 \end{aligned}\right], \tag{11}$$

$$\frac{\partial u_{pv}}{\partial \eta_1}+\frac{\partial v_{pv}}{\partial \eta_2}=0, \tag{12}$$

$$\rho_f c_m\left[\frac{\partial u_{pv}}{\partial t}+u_{pv}\frac{\partial u_{pv}}{\partial \eta_1}+v_{pv}\frac{\partial u_{pv}}{\partial \eta_2}\right]=-c_m\frac{\partial p}{\partial \eta_1}+D_f c_m\left(u_{fv}-u_{pv}\right), \tag{13}$$

$$\rho_f c_m\left[\frac{\partial v_{pv}}{\partial t}+u_{pv}\frac{\partial v_{pv}}{\partial \eta_1}+v_{pv}\frac{\partial v_{pv}}{\partial \eta_2}\right]=-c_m\frac{\partial p}{\partial \eta_2}+D_f c_m\left(v_{fv}-v_{pv}\right), \tag{14}$$

The boundary conditions are

$$u_{fv}\left(\eta_2=h\right)=-l\left(1+\frac{1}{N_p}\right)\left(\frac{\partial u_{fv}}{\partial \eta_2}+\frac{\partial v_{fv}}{\partial \eta_1}\right),\ u_{fv}\left(\eta_2=-h\right)=l\left(1+\frac{1}{N_p}\right)\left(\frac{\partial u_{fv}}{\partial \eta_2}+\frac{\partial v_{fv}}{\partial \eta_1}\right), \tag{15}$$

$$T_{f,p}\left(\eta_2=-h\right)=T_0+k_1\left(\frac{\partial T_{f,p}}{\partial \eta_2}\right),\ T_{f,p}\left(\eta_2=h\right)=T_1-k_1\left(\frac{\partial T_{f,p}}{\partial \eta_2}\right). \tag{16}$$

The dimensionless quantities are

$$\left.\begin{aligned}
&\bar{\eta}_1=\frac{\eta_1}{\lambda},\quad \bar{\eta}_2=\frac{\eta_2}{a},\quad \bar{u}_{fv}=\frac{u_{fv}}{u_0},\quad \bar{u}_{pv}=\frac{u_{pv}}{u_0},\quad \bar{v}_{fv}=\frac{v_{fv}}{\delta u_0},\quad \bar{v}_{pv}=\frac{v_{pv}}{\delta u_0},\ \chi_1=\frac{k_1}{a},\bar{h}=\frac{h}{a},\\
&\bar{p}=\frac{a\delta p}{u_0\mu_s},\quad \beta=\frac{b}{a},\quad \chi_2=\frac{l}{a},\quad \bar{\Phi}=\frac{\Phi}{\zeta},\quad \delta=\frac{a}{\xi},Br=\frac{u_0\mu_s}{K\left(T_1-T_0\right)}\quad U_{hs}=\frac{-\varepsilon\zeta E_{\eta_1}}{u_0\mu_s},\\
&\Lambda=aez\sqrt{\frac{2n_o}{\varepsilon h_b T_m}},\quad Ha=aB_o\sqrt{\frac{\sigma}{\mu_s}},\bar{T}_{f,p}=\frac{T_{f,p}-T_0}{T_1-T_0}
\end{aligned}\right\}. \tag{17}$$

After removing the bars, the dimensionless form of the given problem is given by

$$\frac{\partial u_{fv}}{\partial \eta_1}+\frac{\partial v_{fv}}{\partial \eta_2}=0, \tag{18}$$

$$\left(1+\frac{1}{N_p}\right)\frac{\partial^2 u_{fv}}{\partial {\eta_2}^2}-\frac{H\alpha^2}{(1-c_m)}u_{fv}-\frac{\Lambda^2 u_{hs}}{(1-c_m)}\frac{\cosh\left[\Lambda\eta_2\right]}{\cosh\left[\Lambda h\right]}-\frac{1}{(1-c_m)}\frac{\partial p}{\partial \eta_1}=0, \tag{19}$$

$$\frac{\partial p}{\partial \eta_2}=0, \tag{20}$$

$$\frac{\partial^2 T_{f,p}}{\partial {\eta_2}^2}+Br\left(1+\frac{1}{N_p}\right)\left(\frac{\partial u_{fv}}{\partial \eta_2}\right)^2=0, \tag{21}$$

$$\frac{\partial u_{pv}}{\partial \eta_1}+\frac{\partial v_{pv}}{\partial \eta_2}=0, \tag{22}$$

$$\frac{\mu_s}{a\delta\xi}\frac{\partial p}{\partial \eta_1} = D_f\left(u_{fv} - u_{pv}\right). \tag{23}$$

$$\frac{\partial p}{\partial \eta_2} = 0, \tag{24}$$

The boundary conditions are

$$u_{fv}\left(\eta_2 = h\right) = -\chi_1\left(1+\frac{1}{N_p}\right)\left(\frac{\partial u_{fv}}{\partial \eta_2}\right),\ u_{fv}\left(\eta_2 = -h\right) = \chi_1\left(1+\frac{1}{N_p}\right)\left(\frac{\partial u_{fv}}{\partial \eta_2}\right), \tag{25}$$

$$T_{f,p}\left(\eta_2 = -h\right) = \chi_2\left(\frac{\partial T_{f,p}}{\partial \eta_2}\right),\ T_{f,p}\left(\eta_2 = h\right) = 1-\chi_2\left(\frac{\partial T_{f,p}}{\partial \eta_2}\right). \tag{26}$$

where $$h(\eta_1) = \begin{cases} 1-\Gamma\sin^2\left(\pi\eta_1\right) & \text{When } 0.5 < \eta_1 < 1.5 \\ 0.5 & \text{Othwewise.} \end{cases}. \tag{27}$$

Solving the above equations, we get the closed-form solution as

$$u_{fv} = -\cosh\left[\eta_2\sqrt{A_1}\right]\left(\frac{\left(\frac{\partial p}{\partial \eta_1}\right)N_p A_4 + \left(N_p\cosh\left[h\Lambda\right] + \Lambda\left(1+N_p\right)\chi_1\sinh\left[h\Lambda\right]\right)A_5}{N_p\cosh\left[h\sqrt{A_1}\right] + \left(1+N_p\right)\chi_1\sinh\left[h\sqrt{A_1}\right]\sqrt{A_1}}\right), \tag{28}$$
$$+\left(\frac{\partial p}{\partial \eta_1}\right)A_4 + A_5\cosh\left[\Lambda\eta_2\right],$$

$$u_{pv} = \left(\begin{array}{c} -\cosh\left[\eta_2\sqrt{A_1}\right]\left(\frac{\left(\frac{\partial p}{\partial \eta_1}\right)N_p A_4 + \left(\begin{array}{l} N_p\cosh\left[h\Lambda\right] \\ +\Lambda\left(1+N_p\right)\chi_1\sinh\left[h\Lambda\right] \end{array}\right)A_5}{N_p\cosh\left[h\sqrt{A_1}\right] + \left(1+N_p\right)\chi_1\sinh\left[h\sqrt{A_1}\right]\sqrt{A_1}}\right) \\ +\left(\frac{\partial p}{\partial \eta_1}\right)A_4 + A_5\cosh\left[\Lambda\eta_2\right] \end{array}\right) - \frac{\mu_s}{a\delta\xi D_f}\left(\frac{\partial p}{\partial \eta_1}\right), \tag{29}$$

The total volumetric flow rate is defined by

$$Q = \int_{-h}^{h} u_{fv}\,d\eta_2 + \int_{-h}^{h} u_{pv}\,d\eta_2, \tag{30}$$

$$Q=\begin{pmatrix} -\dfrac{4\sinh\left[h\sqrt{A_1}\right]\left(\left(\dfrac{\partial p}{\partial \eta_1}\right)N_p A_4+\begin{pmatrix}N_p\cosh[h\Lambda]\\ +\Lambda\left(1+N_p\right)\chi_1\sinh[h\Lambda]\end{pmatrix}A_5\right)}{N_p\cosh\left[h\sqrt{A_1}\right]\sqrt{A_1}+\left(1+N_p\right)\chi_1\sinh\left[h\sqrt{A_1}\right]A_1} \\ -\dfrac{2h\left(\dfrac{\partial p}{\partial \eta_1}\right)\mu_s}{aD_f\delta\xi}+4h\left(\dfrac{\partial p}{\partial \eta_1}\right)A_4+\dfrac{4\sinh[h\Lambda]A_5}{\Lambda} \end{pmatrix}. \tag{31}$$

Solving the above equation for $\partial p/\partial \eta_1$ is obtain as

$$\partial p/\partial \eta_1=\frac{-Q+\dfrac{4\sinh[h\Lambda]A_5}{\Lambda}-\dfrac{4\left(N_p\cosh[h\Lambda]+\Lambda\left(1+N_p\right)\chi_1\sinh[h\Lambda]\right)\sinh\left[h\sqrt{A_1}\right]A_5}{N_p\cosh\left[h\sqrt{A_1}\right]\sqrt{A_1}+\left(1+N_p\right)\chi_1\sinh\left[h\sqrt{A_1}\right]A_1}}{-4hA_4+\dfrac{4N_p\sinh\left[h\sqrt{A_1}\right]A_4}{N_p\cosh\left[h\sqrt{A_1}\right]\sqrt{A_1}+\left(1+N_p\right)\chi_1\sinh\left[h\sqrt{A_1}\right]A_1}+\dfrac{2h\mu_s}{aD_f\delta\xi}}. \tag{32}$$

The stream function is calculated form $u_{fv}=\partial\psi/\partial\eta_2$ and expressed by

$$\psi=\left(\frac{\partial p}{\partial \eta_1}\right)\eta_2 A_4+\frac{\sinh[\Lambda\eta_2]A_5}{\Lambda}-\frac{\sinh\left[\eta_2\sqrt{A_1}\right]\left(\left(\dfrac{\partial p}{\partial \eta_1}\right)N_p A_4+\begin{pmatrix}N_p\cosh[h\Lambda]\\ +\Lambda\left(1+N_p\right)\chi_1\sinh[h\Lambda]\end{pmatrix}A_5\right)}{N_p\cosh\left[h\sqrt{A_1}\right]\sqrt{A_1}+\left(1+N_p\right)\chi_1\sinh\left[h\sqrt{A_1}\right]A_1} \tag{33}$$

The closed-form solution of heat equations is defined by

$$\begin{aligned}T_{f,p}=&A_7\cosh[2\Lambda\eta_2]+A_8\cosh\left[2\eta_2\sqrt{A_1}\right]+A_9\cosh[\Lambda\eta_2]\cosh\left[\eta_2\sqrt{A_1}\right]\\&+A_{10}\sinh[\Lambda\eta_2]\sinh\left[\eta_2\sqrt{A_1}\right]+A_{11}{\eta_2}^2+A_{12}\eta_2+A_{13}\end{aligned} \tag{34}$$

The heat transfer rate is obtained and presented in the following analytical form

$$\begin{aligned}H_{tr}=&2\Lambda\sinh[2h\Lambda]A_7+2\sinh\left[2h\sqrt{A_1}\right]\sqrt{A_1}A_8+\cosh[h\Lambda]\sinh\left[h\sqrt{A_1}\right]\left(\sqrt{A_1}A_9+\Lambda A_{10}\right)\\&+\cosh\left[h\sqrt{A_1}\right]\sinh[h\Lambda]\left(\Lambda A_9+\sqrt{A_1}A_{10}\right)+2hA_{11}+A_{12}\end{aligned}. \tag{35}$$

The constants $A_1, A_2, ..., A_{13}$ are defined as.

$$A_1=\frac{Ha^2}{\left(1-c_m\right)\left(1+\dfrac{1}{N_p}\right)}, A_2=\left(1+\frac{ac_mD_f}{\left(1-c_m\right)\delta\xi D_f}\right)\frac{1}{\left(1+\dfrac{1}{N_p}\right)},$$

$$A_3=\frac{\Lambda^2 u_{hs}}{\left(1+\frac{1}{N_p}\right)\left(1-c_m\right)\cosh\left[\Lambda h\right]},A_4=-\frac{A_2}{A_1},A_5=\frac{A_3}{\Lambda^2-A_1},$$

$$A_6=\left(\frac{\left(\partial p/\partial \eta_1\right)N_pA_4+\left(N_p\cosh\left[h\Lambda\right]+\Lambda\left(1+N_p\right)\chi_1\sinh\left[h\Lambda\right]\right)A_5}{N_p\cosh\left[h\sqrt{A_1}\right]+\left(1+N_p\right)\chi_1\sinh\left[h\sqrt{A_1}\right]\sqrt{A_1}}\right),A_7=-\frac{Br\left(1+N_p\right)A_5^2}{8N_p},A_8=-\frac{Br\left(1+N_p\right)A_6^2}{8N_p},$$

$$A_9=-\frac{4Br\Lambda^2\left(1+N_p\right)A_1A_5A_6}{N_p\left(\Lambda^2-A_1\right)^2},A_{10}=\frac{2Br\Lambda\left(1+N_p\right)\sqrt{A_1}\left(\Lambda^2+A_1\right)A_5A_6}{N_p\left(\Lambda^2-A_1\right)^2},A_{11}=\frac{Br\left(1+N_p\right)\left(\Lambda^2A_5^2+A_1A_6^2\right)}{4N_p},$$

$$A_{12}=\frac{1}{2h+\chi_1+\chi_2}\left(1+\left(\chi_1-\chi_2\right)\left(\begin{matrix}-2\Lambda\sinh\left[2h\Lambda\right]A_7-\cosh\left[h\Lambda\right]\sinh\left[h\sqrt{A_1}\right]\left(\sqrt{A_1}A_9+\Lambda A_{10}\right)\\-\cosh\left[h\sqrt{A_1}\right]\sinh\left[h\Lambda\right]\left(\Lambda A_9+\sqrt{A_1}A_{10}\right)-2\left(\sinh\left[2h\sqrt{A_1}\right]\sqrt{A_1}A_8+hA_{11}\right)\end{matrix}\right)\right),$$

$$A_{13}=\frac{1}{2h+\chi_1+\chi_2}\left(\begin{matrix}h+\chi_2+\left(-\left(2h+\chi_1+\chi_2\right)\cosh\left[2h\Lambda\right]-2\Lambda\left(2\chi_1\chi_2+h\left(\chi_1+\chi_2\right)\right)\sinh\left[2h\Lambda\right]\right)A_7\\+\left(-\left(2h+\chi_1+\chi_2\right)\cosh\left[2h\sqrt{A_1}\right]-2\left(2\chi_1\chi_2+h\left(\chi_1+\chi_2\right)\right)\sinh\left[2h\sqrt{A_1}\right]\sqrt{A_1}\right)A_8\\+\sinh\left[h\sqrt{A_1}\right]\left(-\left(2h+\chi_1+\chi_2\right)\sinh\left[h\Lambda\right]A_{10}-\left(2\chi_1\chi_2+h\left(\chi_1+\chi_2\right)\right)\cosh\left[h\Lambda\right]\left(\sqrt{A_1}A_9+\Lambda A_{10}\right)\right)\\+\cosh\left[h\sqrt{A_1}\right]\left(-\left(2h+\chi_1+\chi_2\right)\cosh\left[h\Lambda\right]A_9-\left(2\chi_1\chi_2+h\left(\chi_1+\chi_2\right)\right)\sinh\left[h\Lambda\right]\left(\Lambda A_9+\sqrt{A_1}A_{10}\right)\right)\\-h\left(2h^2+4\chi_1\chi_2+3h\left(\chi_1+\chi_2\right)\right)A_{11}\end{matrix}\right)$$

5. Results and Discussion

The hydromagnetic fluid and particle suspension model is developed in this theoretical study and discusses heat transfer analysis through the energy equation. The governing equations of non-Newtonian fluid (i.e. Casson fluid) are solved and presented as the closed-form solution of the problem in section two and MATHEMATICA code is developed to construct the graphs. This section is included here to observe the physical interpretation of emerging parameters namely, the non-Newtonian parameter $\left(N_p\right)$, the velocity slip parameter $\left(\chi_1\right)$, the electro-osmotic parameter $\left(\Lambda\right)$, the coefficient of particle fraction $\left(c_m\right)$, the Helmholtz–Smoluchowski velocity $\left(u_{hs}\right)$, the Hartman number $\left(Ha\right)$, the thermal slip parameter $\left(\chi_2\right)$, and Brinkman number $\left(Br\right)$ on the fluid and particle velocities profiles, the temperature distribution, the stream function, and the heat transfer rate for the suitable range. To observe these physical interpretations, the authors construct **Figures 2** to **14** and one table.

Figure 2 explains the effects of non-Newtonian parameter $\left(N_p\right)$ on fluid and particle velocity distribution for a suitable range. In this figure, the left and right figures indicate the fluid and particle phase velocities. Here, the increasing behavior of both velocities is observed against the

non-Newtonian parameter. Physically it means that the non-Newtonian parameter $\left(N_p\right)$ enhancing the plastic dynamic viscosity of fluid that contributes to diminishing the values of yield stress as a result, the velocity is reduced against the non-Newtonian parameter $\left(N_p\right)$. The results of these figures also revealed that the magnitude of the particulate velocity is higher than the velocity of the fluid phase. The effect of the velocity parameter χ_1 on fluid and particulate velocity distribution is reported in **Figure 3**. Since it is well known when slip exists then their velocity is not zero at the walls of the channel or the velocity of fluid is not equal to the velocity of adjacent walls of the channel. It can also be explained as the difference between fluid velocity and adjusted walls of velocity is not zero. This figure reported the decreasing trend in fluid velocity against the velocity slip parameter χ_1 in the interval $0.0 \le \eta_1 \le 0.8$ and $1.2 \le \eta_1 \le 2.0$ but a converse relation is observed in the interval $0.8 \le \eta_1 \le 1.2$. A similar trend is observed in particulate velocity. The physical reason for decreasing the velocity distribution is that the entire force is not transferred through the walls of the channel inside Casson fluid. The influence of electro-osmotic parameter Λ on both velocities is illustrated in **Figure 4**. This parameter is inversely proportional to the Daybe length parameter i.e. $\Lambda = aez\sqrt{\frac{2n_0}{\varepsilon h_b T_m}} = \frac{a}{\lambda_D}, \lambda_D \propto \frac{1}{\Lambda}$. The electro-osmotic parameter promotes the fluid and particulate velocity distribution remarkably. The electro-osmotic body force will vanish when $\Lambda \to 0$. The impact of particle fraction coefficient c_m is highlighted in fluid and particulate velocities in **Figure 5**. It is interesting to note that the particle fraction coefficient c_m boosts the velocities distribution and the problem can be achieved in a single for $c_m \to 0$. The physical reason is that the drag force between the fluid and particle phase diminishes by increasing the values of the particle fraction coefficient as a result the momentum of the fluid speeds up. **Figure 6** demonstrates the effects of the Helmholtz–Smoluchowski velocity on fluid and particulate velocity distribution. In this figure, the left figure indicates the fluid velocity while the right one shows the particle velocity. Here, we observed that this parameter promotes the fluid and particle phase velocities extensively. Another important parameter of this study is the Hartman number. It is described from **Figure 7**, that the decrement in velocity distribution is noted for increasing the values of the Hartmann number. From equation (17), $Ha = aB_0\sqrt{\frac{\sigma}{\mu_s}}$ which indicates the relationship between the hydromagnetic force and magnetic body force which means that greater Lorentz force is produced against the greater transverse magnetic force that causes the decreasing behavior in the velocity profile. Similar results are observed in particle phase velocity. From these figures, we can say that the velocities can be controlled by increasing or decreasing the strength of the magnetic field. The streamlines are drawn in **Figures 8** to **10** against the particle fraction coefficient, velocity slip parameter, and non-Newtonian parameter, respectively. The number of streamlines increases due to the contribution of the particle fraction coefficient i.e. for non-zero values of c_m the motion of the fluid particle increases and the values of stream function vary from $\psi = 44.8$ to $\psi = 46.2$ for $c_m = 0.0$ to $c_m = 0.4$, which is shown in **Figure 8**. A similar behavior of the stream function is observed against the velocity slip parameter and this case the stream function gets the values of $\psi = 43.4$ to $\psi = 46.2$ for $\chi_1 = 0.0$ to $\chi_1 = 0.5$ (see **Figure 9**).

The strength of the stream function reducing against the non-Newtonian parameter i.e. the stream function covers a larger area of the channel for the case of Newtonian fluid i.e. $N_p \to \infty$ as compared to Casson fluid i.e. $N_p = 0.1$. Moreover, the stream function gets the values of $\psi = 46.9$ and $\psi = 42.7$ for Newtonian and non-Newtonian fluid, respectively (see **Figure 10**).

The variation of temperature distribution against non-Newtonian parameter N_p, the coefficient of particle fraction c_m, the velocity slip parameter χ_1, the thermal slip parameter χ_2, the electro-osmotic parameter Λ, the Helmholtz–Smoluchowski velocity, Brinkman number Br and the Hartman number are shown in **Figures 11-14**, respectively. The non-Newtonian parameter diminishes the temperature profile which is illustrated in **Figure 11 (left)** and this reduction in temperature appears due to diminishing the values of yield stress against enhancing the plastic dynamic viscosity of fluid due to the non-Newtonian parameter. The particle fraction coefficient c_m enhancing the temperature distribution this observation is shown in **Figure 11 (right)** and it is happening due to the collision of solid particles that are responsible for enhancing the temperature distribution. **Figure 12** portrays the effects of velocity and thermal slip parameters. From these figures, it is observed that the velocity slip parameter diminishes the temperature profiles (see **Figure 12(left)**) while the thermal slip parameter updates the temperature distribution (see **Figure 12(right)**). The variation of temperature distribution via electro-osmotic parameter and the Helmholtz–Smoluchowski velocity are displayed in **Figure 13** and both parameters enhance the temperature profile. The effects of the Brinkman number and Hartman number on the temperature profile are depicted in **Figure 14**. From the left figure of **14**, it is observed that the Brinkman number increases the temperature distribution because the Brinkman number is coming from viscous dissipation that increases the temperature profile. On the other hand, the Hartman number reduces the temperature, and it is happening due to the reduction of the kinetic energy for increasing the Hartman number (see **Figure 14 (right)**).

The most important quantity of this investigation is the heat transfer rate (H_{tr}) and variation of heat transfer rate against the non-Newtonian parameter (N_p), the velocity slip parameter (χ_1), the electro-osmotic parameter (Λ), the coefficient of particle fraction (c_m), the Helmholtz–Smoluchowski velocity (u_{hs}), the Hartman number (Ha), the thermal slip parameter (χ_1), and Brinkman number (Br) is presented in **Table 1**. The computational results listed in Table 1 revealed that the heat transfer rate is increased against the thermal slip parameter (χ_2) the electro-osmotic parameter (Λ), Brinkman number (Br) and the Helmholtz–Smoluchowski velocity (u_{hs}) while its decreasing behavior is noted against the non-Newtonian parameter (N_p), the velocity slip parameter (χ_1), the coefficient of particle fraction (c_m), and the Hartman number (Ha).

6. Validation part

The results are validated by the study of Hussain et al. [31] for limiting cases. In [31], the authors discussed the theoretical analysis of electro osmotic flow of multiphase flow through convergent, divergent, and nozzle type of channels under the act of the constant magnetic force. They

considered the Newtonian fluid as a base fluid and hafnium nanoparticles were suspended in the base fluid and performed the momentum analysis. We have validated our study with geometry two (divergent channel) of Hussain et al. [31] for setting $N_p \to \infty$ and $\chi_1 \to 0$. The results of both studies are shown in **Figure 15** and noted good agreement with each other.

7. Conclusion

A mathematical study of fluid and particle suspension in Casson rheological is reported here to examine the heat transfer analysis in divergent channels under the effects of electroosmotic and magnetic forces. The velocity and thermal slip conditions are also considered. The electro-osmotic phenomena are modeled through the Poisson equation and solved this equation by using the Hückel linearization method. The current study presented innovative, valuable physical data and calculated the accurate exact solution. The important results of this investigation are.

1. The exact solution of fluid-suspension in Casson rheological fluid is obtained with Hafnium particles.
2. The fluid-particle phase velocities and temperature distribution are decreasing against the velocity slip parameter and Hartman number.
3. The thermal slip parameter upgrades the temperature distribution.
4. The non-Newtonian parameter controls the motion of fluid and particle phase velocities and temperature distribution.
5. The heat transfer rate is a decreasing function of the non-Newtonian parameter, velocity slip parameter, Hartman number, and coefficient of particle fraction while this behavior no longer exists against the thermal slip parameter, Brinkman number, the Helmholtz–Smoluchowski velocity, and electroosmotic parameter.
6. The current fluid-particle suspension Casson model helps understand the thermal properties of such a model under the action of the electric and magnetic field with slip boundary conditions.
7. The suspension of dense particles can be useful in solar power plants to restore more energy.

Data Availability Statement

No Data is associated with the manuscript.

Table 1: The variation of the average Nusselt number against the following parameters.

N_p	χ_1	χ_2	Λ	c_m	Br	u_{hs}	Ha	H_{tr}	Behavior
1.0	0.01	0.01	1.0	0.1	1.0	1.0	2.0	1.3852	Decreasing
3.0	---	---	---	---	---	---	---	0.7179	
2.0	0.02	---	---	---	---	---	---	0.6035	Decreasing
---	0.03	---	---	---	---	---	---	0.3775	
---	0.015	0.02	---	---	---	---	---	0.7656	Increasing
---	---	0.03	---	---	---	---	---	0.7914	
---	---	0.015	3.0	---	---	---	---	0.7874	Increasing
---	---	---	5.0	---	---	---	---	0.9529	

---	---	---	1.0	0.2	---	---	---	0.7512	Decreasing
---	---	---	---	0.3	---	---	---	0.7492	
---	---	---	---	0.1	1.5	---	---	1.6144	Increasing
---	---	---	---	---	2.0	---	---	2.4762	
---	---	---	---	---	1.0	2.0	---	0.7529	Increasing
---	---	---	---	---	---	5.0	---	0.7536	
---	---	---	---	---	---	1.0	1.0	0.7669	Decreasing
---	---	---	---	---	---	---	3.0	0.7338	

References

1. Mahanthesh, B., & Gireesha, B. J., "Scrutinization of thermal radiation, viscous dissipation and Joule heating effects on Marangoni convective two-phase flow of Casson fluid with fluid-particle suspension", *Results in phys*, **8**, pp. 869-878 (2018).
2. Gireesha, B. J., Mahanthesh, B., et al. "Mixed convection two-phase flow of Maxwell fluid under the influence of non-linear thermal radiation, non-uniform heat source/sink and fluid-particle suspension", *Ain Shams Eng J*, **9**(4), pp. 735-746(2018).
3. Saffman, P. G., "On the stability of laminar flow of a dusty gas, *Journal of fluid mechanics*, **13**(1), pp. 120-128 (1962).
4. Bhatti, M. M., Zeeshan, A., & Ellahi, R., "Heat transfer analysis on peristaltically induced motion of particle-fluid suspension with variable viscosity: clot blood model", *Comput methods Programs Biomed*, **137**, pp. 115-124(2016).
5. Bhatti, M. M., Zeeshan, A., & Rashidi, M. M., "Influence of magnetohydrodynamics on metachronal wave of particle-fluid suspension due to cilia motion", *Eng Sci Tech Int J*, **20**(1), 265-271(2017).
6. Bhatti, M. M., Zeeshan, A., Ellahi, et al. "Mathematical modeling of heat and mass transfer effects on MHD peristaltic propulsion of two-phase flow through a Darcy-Brinkman-Forchheimer porous medium", *Adv Powder Techno*, **29**(5), 1189-1197(2018).
7. Nazeer, M., Hussain, F., Ahmad, F., et al. "Multi-phase flow of Jeffrey fluid bounded within magnetized horizontal surface" *Surf Interfaces*, **22**, pp. 100846(2021).
8. Nazeer, M., Hussain, F., Ahmad, F., et al. "Numerical analysis of multiphase flow of couple stress fluid thermally effected by moving surface", *Int J Mod Phys B*, **35**(18), pp. 2150188(2021).
9. Nazeer, M., Khan, M. I., Chu, Y. M., et al. "Mathematical modeling of multiphase flows of third-grade fluid with lubrication effects through an inclined channel: analytical treatment", *J Dispers Sci Technol*, **43**(10), pp. 1555-1567(2022).
10. Kumar, K. G., Rudraswamy, N. G., Gireesha, B. J., et al. "Non linear thermal radiation effect on Williamson fluid with particle-liquid suspension past a stretching surface", *Results Phys*, **7**, pp. 3196-3202(2017).
11. Pavithra, G. M., & Gireesha, B. J., "Unsteady flow and heat transfer of a fluid-particle suspension over an exponentially stretching sheet", Ain *Shams Eng J*, **5**(2), pp. 613-624(2014).
12. Hatami, M., Hosseinzadeh, K., Domairry, G., et al. "Numerical study of MHD two-phase Couette flow analysis for fluid-particle suspension between moving parallel plates", *J Taiwan Inst Chem Eng*, **45**(5), pp. 2238-2245(2014).

13. Jha, B. K., & Apere, C. A., "Unsteady MHD two-phase Couette flow of fluid–particle suspension", *Appl Math Model*, **37**(4), pp. 1920-1931(2013).
14. Jha, B. K., & Malgwi, P. B., "Computational analysis on unsteady hydromagnetic Couette flow of fluid—Particle suspension in an accelerated porous channel", *Partial Differ Equ Appl Math*, **5**, pp100370(2022).
15. Al-Zubaidi, A., Nazeer, M., Subia, G. S., et al. "Mathematical modeling and simulation of MHD electro-osmotic flow of Jeffrey fluid in convergent geometry", *Waves Random Complex Media*, (2021). https://doi.org/10.1080/17455030.2021.2000672
16. Ge-JiLe, H., Nazeer, M., Hussain, F., et al. "Two-phase flow of MHD Jeffrey fluid with the suspension of tiny metallic particles incorporated with viscous dissipation and porous medium", *Adv Mech Eng*, **13**(3), pp. 1-15 (2021).
17. Zeeshan, A., Hussain, F., Ellahi, R., et al. "A study of gravitational and magnetic effects on coupled stress bi-phase liquid suspended with crystal and Hafnium particles down in steep channel", *J Mol Liq*, **286**, pp. 110898(2019).
18. Ellahi, R., Hussain, F., Asad Abbas, S., et al. "Study of two-phase Newtonian nanofluid flow hybrid with Hafnium particles under the effects of slip", *Inventions*, **5**(1), pp. 6(2020).
19. Bibi, M., Zeeshan, A., & Malik, M. Y., "Numerical analysis of unsteady flow of three-dimensional Williamson fluid-particle suspension with MHD and nonlinear thermal radiations", *Eur Phys J Plus*, **135**, pp. 850(2020).
20. Gad, N. S., "Effect of Hall currents on interaction of pulsatile and peristaltic transport induced flows of a particle–fluid suspension", *Appl Math Comput*, **217**(9), pp. 4313-4320(2011).
21. Chamkha, A. J., "Unsteady laminar hydromagnetic fluid–particle flow and heat transfer in channels and circular pipes", *Int J Heat Fluid Flow*, **21**(6), pp. 740-746 (2000).
22. Ansart, R., García-Triñanes, P., Boissière, B., et al. "Dense gas-particle suspension upward flow used as heat transfer fluid in solar receiver: PEPT experiments and 3D numerical simulations", *Powder Technol*, **307**, pp. 25-36(2017).
23. Spelling, J., Gallo, A., Romero, M., et al. "A high-efficiency solar thermal power plant using a dense particle suspension as the heat transfer fluid", *Energy Procedia*, **69**, pp. 1160-1170(2015).
24. Imran, N., Javed, M., Qayyum, M., et al., "Heat transfer analysis for particle–fluid suspension thermomagnetohydrodynamic peristaltic flow with Darcy–Forchheimer medium", *Heat Transfer*, **50**(4), pp. 3547-3563(2021).
25. Bhatti, M. M., & Zeeshan, A., "Heat and mass transfer analysis on peristaltic flow of particle–fluid suspension with slip effects", *J Mech Med Biol*, **17**(2), pp. 1750028(2017).
26. Nazeer, M., Alqarni, M. Z., Hussain, F., et al. "Computational analysis of multiphase flow of non-Newtonian fluid through inclined channel: heat transfer analysis with perturbation method", *Comput Part Mech*, **10**, pp. 1371-1381(2023).
27. Nazeer, M., Irfan, M., Hussain, F., et al. "Analytical study of heat transfer rate of peristaltic flow in asymmetric channel with laser and magnetic effects: Remedy for autoimmune disease", *Int J Mod Phys B*, **37**(3), pp. 2350025(2023).
28. Nazeer, M., Al-Zubaidi, A., Hussain, F., et al. "Thermal transport of two-phase physiological flow of non-Newtonian fluid through an inclined channel with flexible walls", *Case Stud Therm Eng*, **35**, pp. 102146(2022).

29. Hussain, F., Nazeer, M., Altanji, M., et al. “Thermal analysis of Casson rheological fluid with gold nanoparticles under the impact of gravitational and magnetic forces”, *Case Stud Therm Eng*, **28**, pp. 101433(2021).
30. Xiong, P. Y., Nazeer, M., Hussain, F., et al. “Two-phase flow of couple stress fluid thermally effected slip boundary conditions: Numerical analysis with variable liquids properties”, *Alex Eng J*, **61**(5), pp. 3821-3830(2022).
31. Hussain, F., Ellahi, R., & Zeeshan, A., “Mathematical models of electro-magnetohydrodynamic multiphase flows synthesis with nano-sized hafnium particles”, Appl Sci, **8**(2), pp. 275(2018).
32. Shehzad, N., Zeeshan, A., Shakeel, M., et al. “Effects of magnetohydrodynamics flow on multilayer coatings of Newtonian and non-Newtonian fluids through porous inclined rotating channel”, *Coatings*, **12**(4), pp. 430(2022).
33. Ishtiaq, F., Ellahi, R., Bhatti, M. M. et al. “Insight in thermally radiative cilia-driven flow of electrically conducting non-Newtonian Jeffrey fluid under the influence of induced magnetic field”, *Mathematics*, **10**(12), pp. 2007(2022).
34. Ellahi, R., Sait, S. M., Shehzad, N., et al. “Numerical simulation and mathematical modeling of electro-osmotic Couette–Poiseuille flow of MHD power-law nanofluid with entropy generation”, *Symmetry*, **11**(8), pp. 1038(2019).
35. Nazeer, M., Hussain, F., Hameed, M. K., et al. “Development of mathematical modeling of multi-phase flow of Casson rheological fluid: Theoretical approach”, *Chaos, Soliton Fract*, **150**, pp. 111198(2021).
36. Makinde, O. D., & Gnaneswara Reddy, M., “MHD peristaltic slip flow of Casson fluid and heat transfer in channel filled with a porous medium”, *Sci Iran*, **26**(4), pp. 2342-2355(2019).
37. Ahmad, F., Nazeer, M., Ali, W., et al. “Analytical study on couple stress fluid in an inclined channel”, *Scientia Iranica*, **28**(4), pp. 2164-2175(2021).
38. Khan, A. A., Usman, H., Vafai, K., et al. “Study of peristaltic flow of magnetohydrodynamics Walter's B fluid with slip and heat transfer”, Sci *Iran*, **23**(6), pp. 2650-2662(2016).

Figure 1: The physical sketch of the problem.

Figure 2: Effects of non-Newtonian parameter on fluid and particle phase velocities distribution.

Figure 3: Effects of velocity slip parameter on fluid and particle phase velocities distribution.

Figure 4: Effects of electro-osmotic parameter on fluid and particle phase velocities distribution.

Figure 5: Effects of the coefficient of particle fraction on fluid and particle phase velocities distribution.

Figure 6: Effects of the Helmholtz–Smoluchowski velocity on fluid and particle phase velocities distribution.

Figure 7: Effects of the Hartman number on fluid and particle phase velocities distribution.

Figure 8: The variation of stream function via $c_m = 0$ (left) and $c_m = 0.4$ (right).

Figure 9: The variation of stream function via $\chi_1 = 0$ (left) and $\chi_1 = 0.5$ (right).

Figure 10: The variation of stream function via $N_p = \infty$ (left) and $N_p = 0.1$ (right).

Figure 11: The variation of temperature distribution via non-Newtonian parameter N_p (left) and the coefficient of particle fraction c_m (right).

Figure 12: The variation of temperature distribution via velocity slip parameter χ_1 (left) and the thermal slip parameter χ_2 (right).

Figure 13: The variation of temperature distribution via electro-osmotic parameter Λ (left) and the Helmholtz–Smoluchowski velocity U_{hs} (right).

Figure 14: The variation of temperature distribution via Brinkman number Br (left) and the Hartman number Ha (right).

Figure 15: Solution validation with Hussain et al. [31].

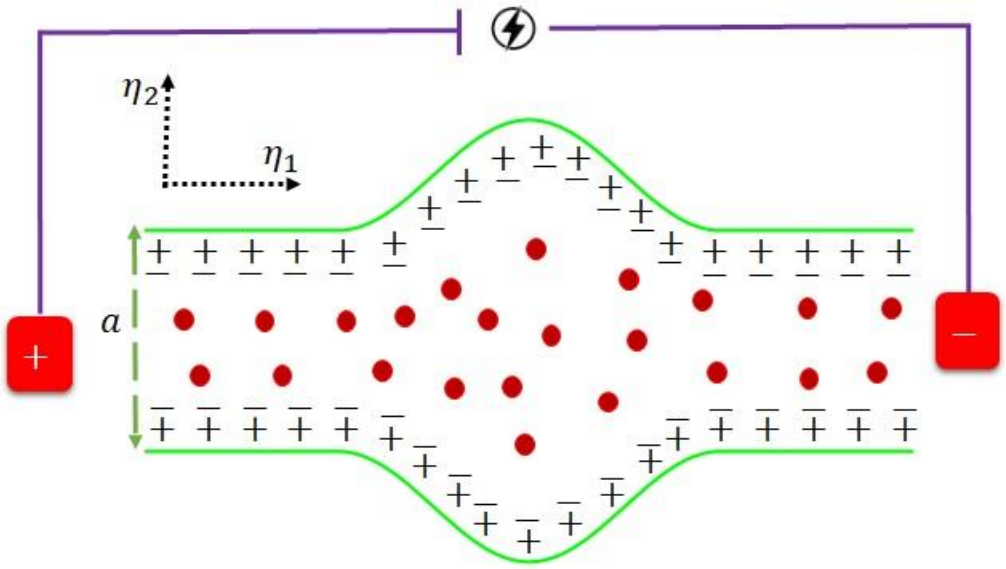

Figure 1

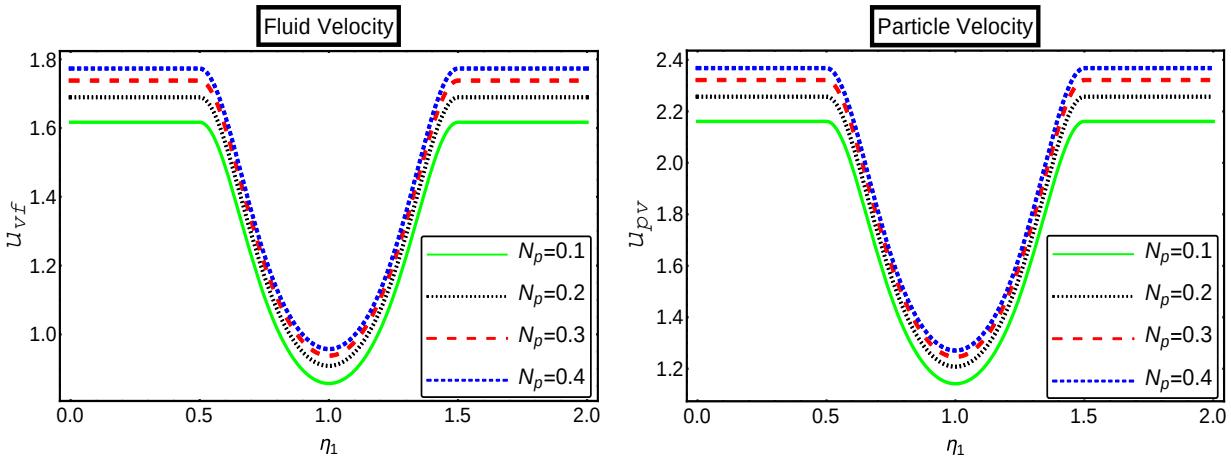

Figure 2

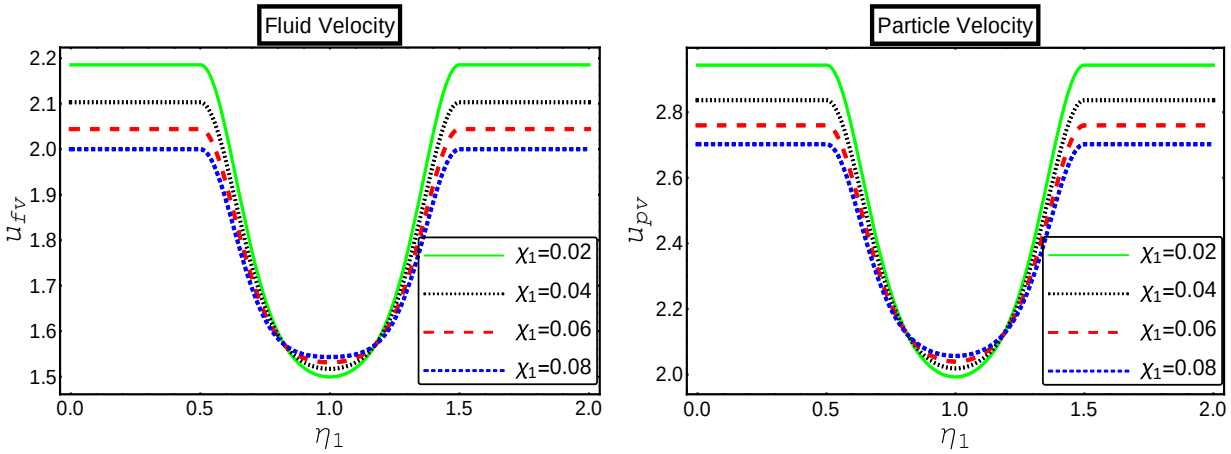

Figure 3

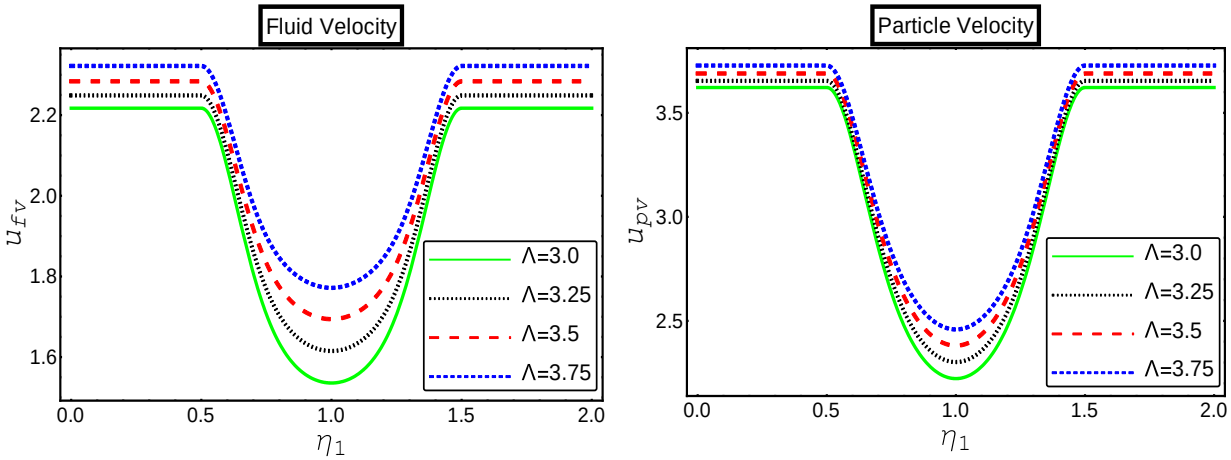

Figure 4

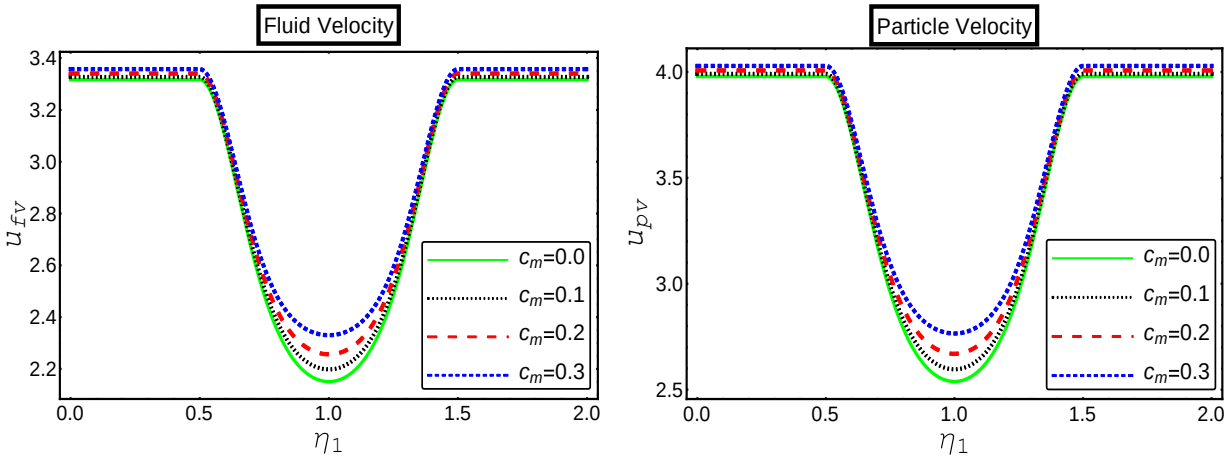

Figure 5

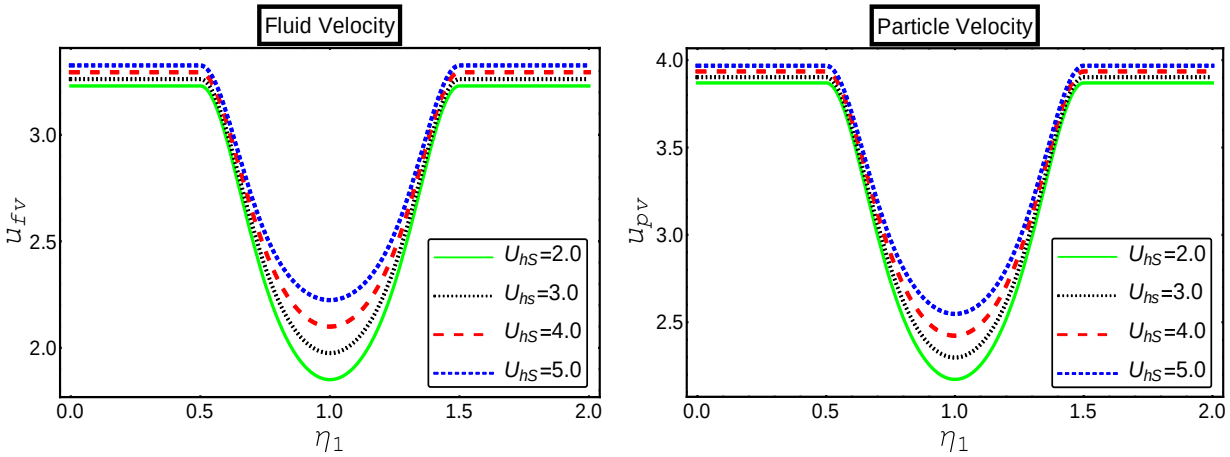

Figure 6

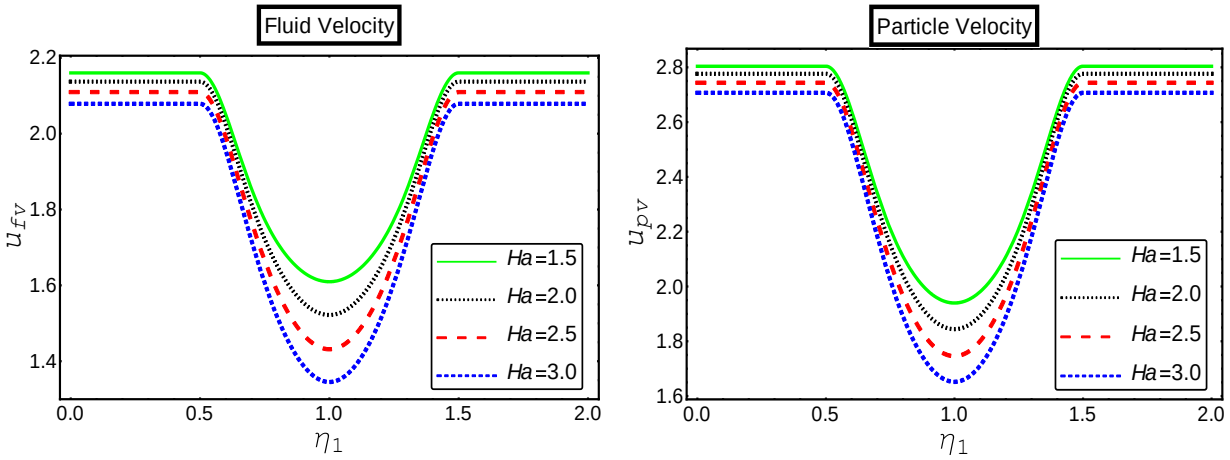

Figure 7

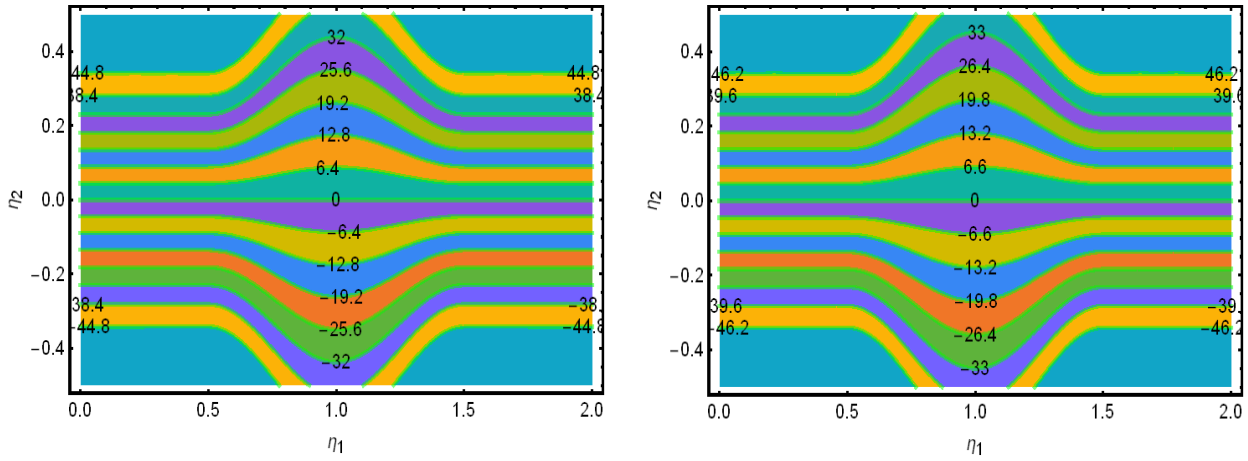

Figure 8

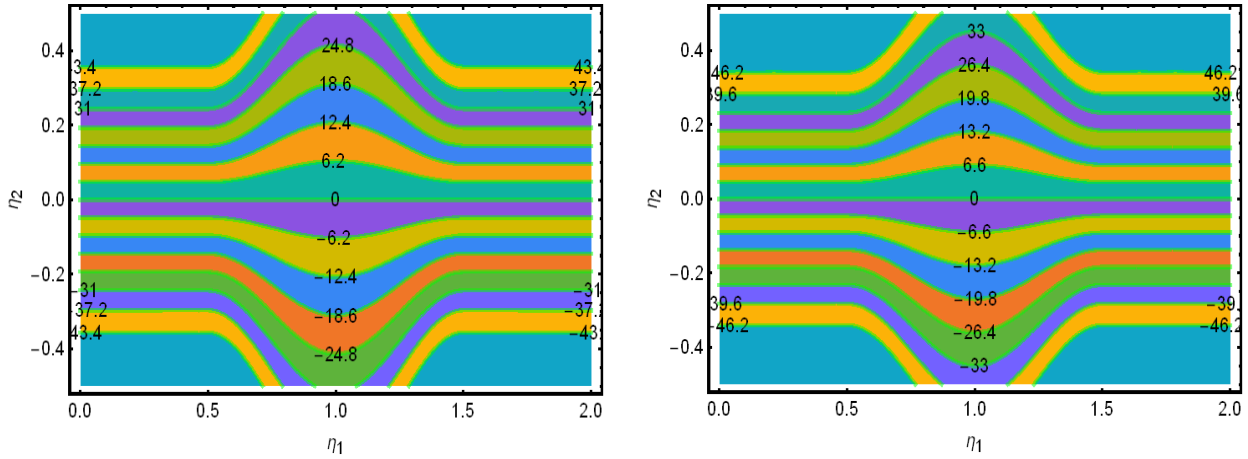

Figure 9

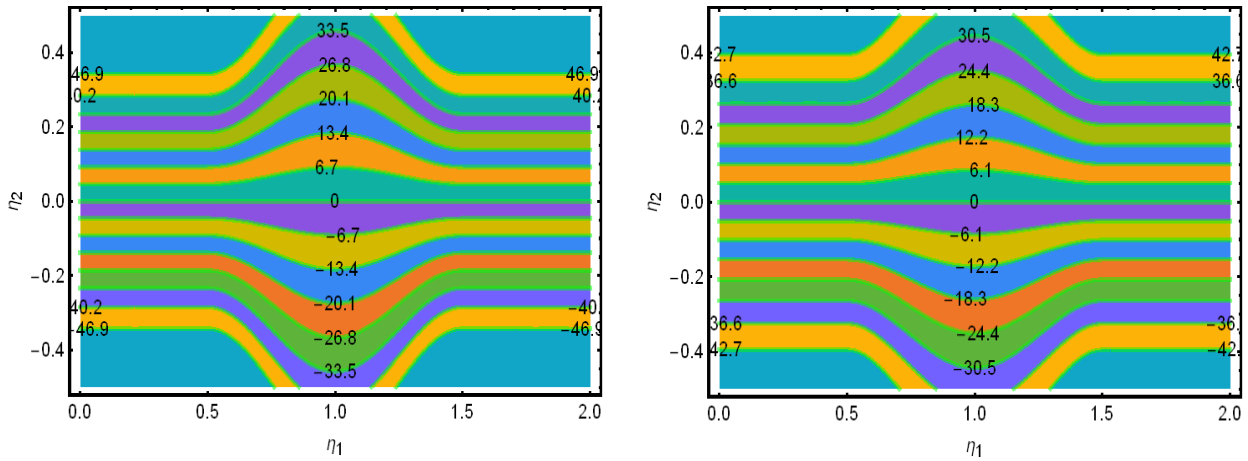

Figure 10

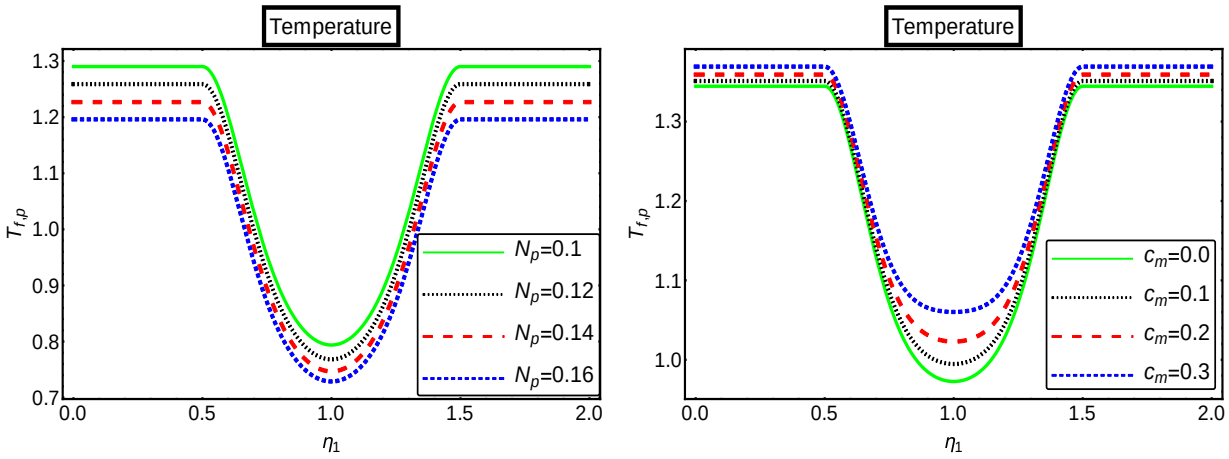

Figure 11

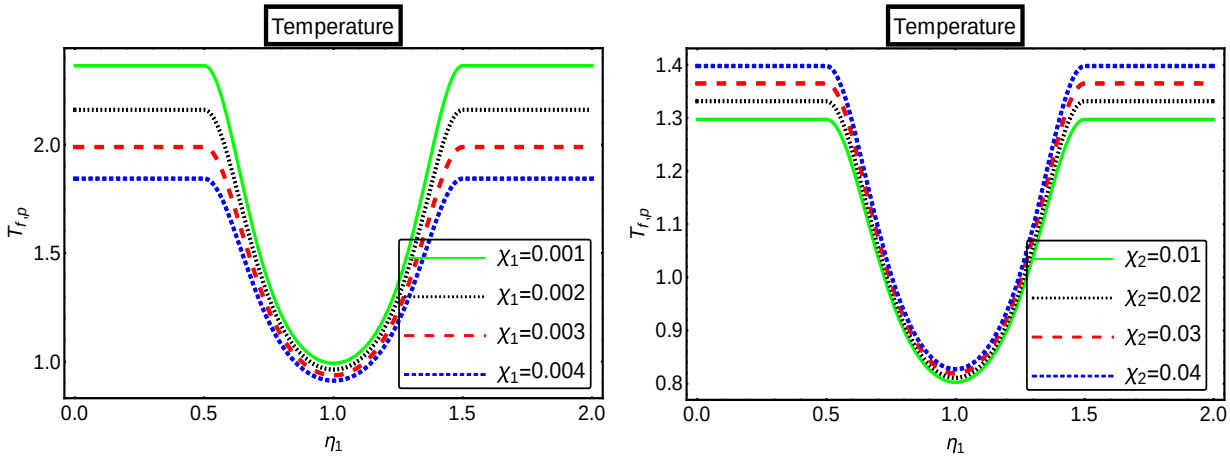

Figure 12

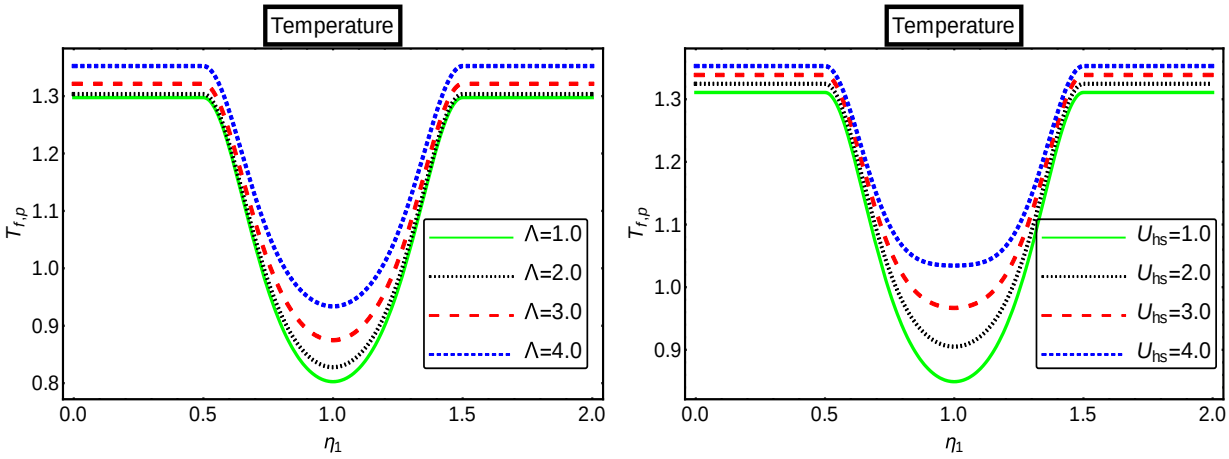

Figure 13

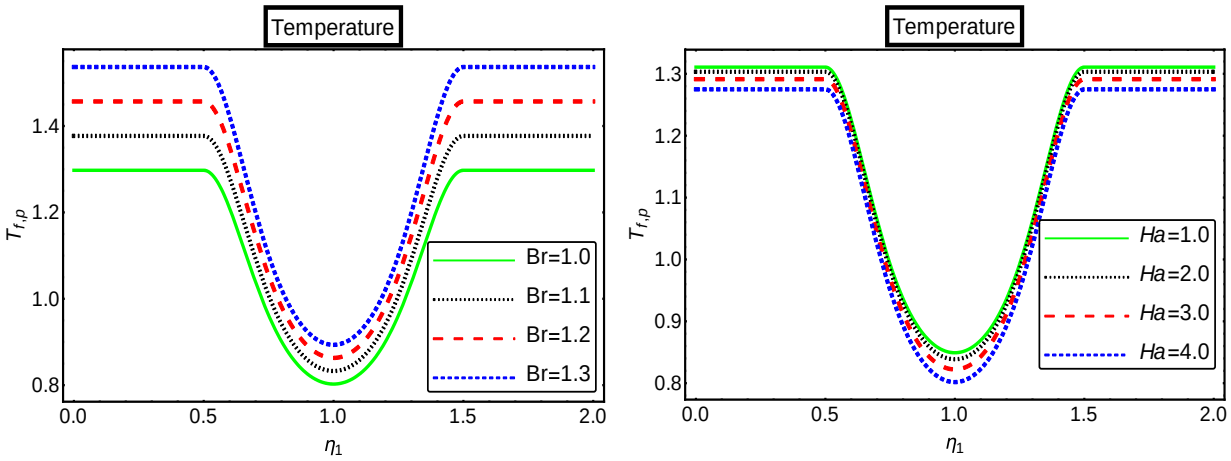

Figure 14

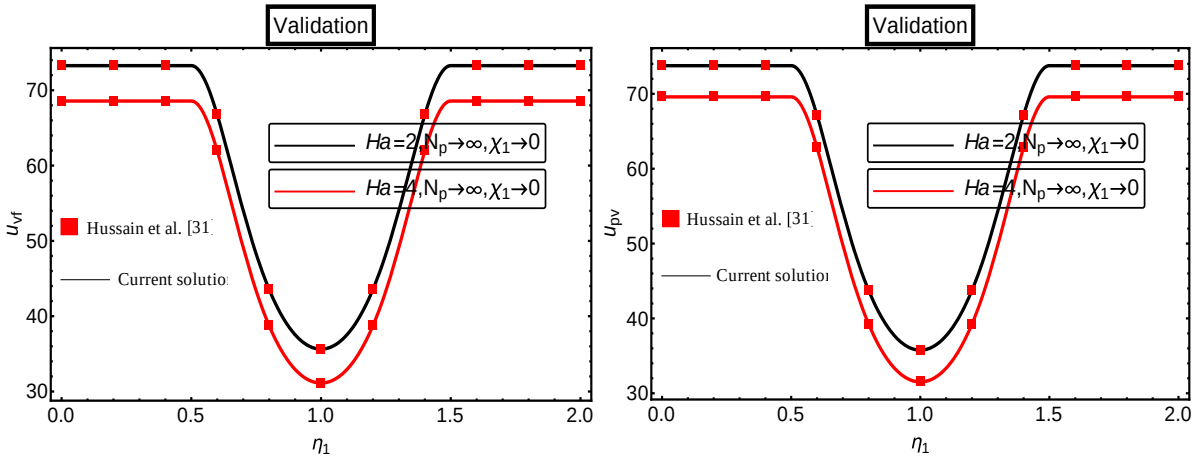

Figure 15

Authors Biography

Dr. Salman Saleem

Salman Saleem received his Ph.D. in Applied Mathematics and is currently working as an Associate Professor at King Khalid University, Abha, Saudi Arabia. His field of research is computational fluid mechanics. He has published a good number of articles in well-reputed journals. He has more than 5500 citations as per the Google Scholar database. He is also serving as an academic and guest editor for various well-known ISI journals. He has received research awards at the national and international levels.

Dr. Mubbashar Nazeer

He completed his doctorate from the Department of Mathematics and Statistics in Applied Mathematics (Fluid Mechanics) at the International Islamic University Islamabad in July 2018. He has served as an Assistant Professor in the Department of Mathematics, Riphah International University Faisalabad Campus near two years. Now, he is working as an Assistant Professor in the Department of Mathematics, Institute of Arts and Sciences, Government College University Faisalabad, Chiniot Campus. His area of research is Cavity flows, Newtonian and non-Newtonian fluids, analytical and numerical methods, Bio-fluid mechanics, porous medium, heat and mass transfer analyses, and Computational Fluid Dynamics. He also received two research awards from national institutions.

M. Waqas Nazir

M. Waqas Nazir is a PhD researcher at the Department of Mathematics and Statistics in Applied Mathematics (Fluid Mechanics), International Islamic University Islamabad. He received a Master of Science (MS) degree in Mathematics from the International Islamic University Islamabad, Pakistan. With the help of both analytical and computational mathematical techniques, his research work focuses on fluid flows related to various industrial applications.

Leema Aliyaru Kunju

Leema Aliyaru Kunju, Indian, a dedicated educator, holds a Master's Degree in Mathematics from the prestigious University of Kerala, India. Since 2011, Leema has been a faculty member at Jazan University, Saudi Arabia, where they currently serve as a Lecturer in Mathematics. With a remarkable 17 years of teaching experience in college classes across India and Saudi Arabia, Leema's expertise encompasses a commitment to enhancing mathematical education for students at every level.